Available online at www.sciencedirect.com
ScienceDirect
Journal of the European Ceramic Society 30 (2010) 1931–1944
www.elsevier.com/locate/jeurceramsoc

Rare-earth element doped Si_3N_4/SiC micro/nano-composites—RT and HT mechanical properties

S. Lojanová [a,*], P. Tatarko [b], Z. Chlup [c], M. Hnatko [a], J. Dusza [b], Z. Lenčéš [a], P. Šajgalík [a]

[a] *Institute of Inorganic Chemistry, Slovak Academy of Sciences, Dúbravská cesta 9, 845 36 Bratislava, Slovakia*
[b] *Institute of Materials Research, Slovak Academy of Sciences, Watsonova 47, 043 53 Košice, Slovakia*
[c] *Institute of Physics of Materials, Academy of Sciences of the Czech Republic, Žižkova 22, 616 62 Brno, Czech Republic*

Received 28 July 2009; received in revised form 11 February 2010; accepted 16 March 2010

Abstract

Dense Si_3N_4/SiC micro/nano-composites with varying grain boundary phase composition were fabricated by hot-pressing under the same conditions. Six different sintering aids (Lu_2O_3, Yb_2O_3, Y_2O_3, Sm_2O_3, Nd_2O_3 and La_2O_3) were used. The formation of SiC nano-inclusions was achieved by *in situ* carbothermal reduction of SiO_2 by C during the sintering process. Room temperature, fracture toughness, hardness and strength tended to increase when the cation radius of the rare-earth element used in the oxide additive decreased (i.e. from La^{3+} to Lu^{3+}). The composite material with Lu_2O_3 sintering additive showed the highest hardness and had reasonably high fracture toughness and strength. The same micro/nano-composite also possessed the highest creep resistance in the temperature range from 1250 °C to 1400 °C and with loads in the range 50–150 MPa.

Keywords: Si_3N_4; SiC; Nano-composites; Fracture toughness; Hardness; Strength; Creep

1. Introduction

Silicon nitride (Si_3N_4) based ceramics are most often used as structural components for high-temperature applications. The high-temperature properties of Si_3N_4 based ceramics strongly depend on the oxide additives used for the densification. The addition of the sintering aids form a low-melting point eutectic liquid with the silica layer present on the surface of starting Si_3N_4 powder particles at the temperature of densification. Resulting amorphous phase present at the multigrain junctions and on the grain boundaries of Si_3N_4 grains dictates the room temperature fracture behaviour of ceramics and also softens at elevated temperatures. This softening leads to the deformation of the ceramic body mainly by grain-boundary sliding. Lot of studies were devoted to the detection of the best combination of sintering additives with respect to the mechanical behaviour of silicon nitride based ceramics.

Satet et al.[1,2] reported the influence of the rare earth (RE)–MgO intergranular phase composition on the room temperature properties of Si_3N_4 ceramics. The room temperature measurements showed that fracture toughness of this class of ceramics increases with increasing ionic radius of RE^{3+} and the four-point bending strength decreases with increasing radius of RE^{3+}. It was found that weaker grain-boundary interface connected with the addition of La^{3+} results in a higher toughness, but in lower strength of the bulk Si_3N_4 material.

Silicon nitride ceramics sintered with the rare-earth oxide additives are also an important class of materials for high-temperature applications because they exhibit good high-temperature strength and thermal shock resistance along with good creep resistance, and high resistance to oxidation.[3–6] It was found that the high-temperature strength of hot-pressed Si_3N_4 ceramic was significantly improved by the addition of Lu_2O_3 additive.[3,7] Besides the high-temperature resistance, also good room temperature properties are required to design material for commercial applications in extreme conditions.

Many studies show that the distribution of fine SiC nano-inclusions in the Si_3N_4 matrix results in improvement of hardness and strength of Si_3N_4/SiC micro/nano-composites. Their presence at grain boundaries hinders the deformation of the composite at the elevated temperatures by the grain-boundary sliding.[8–10]

* Corresponding author.
E-mail address: uachlost@savba.sk (S. Lojanová).

0955-2219/$ – see front matter © 2010 Elsevier Ltd. All rights reserved.
doi:10.1016/j.jeurceramsoc.2010.03.007

Therefore both, incorporation of SiC nano-inclusion to the Si_3N_4 matrix and design of the grain-boundary phase composition can be an effective tool for the tailored room- as well as high-temperature behaviour of Si_3N_4 based ceramic composites.

Present paper deals with the processing of Si_3N_4/SiC micro/nano-composites doped with various rare-earth oxide sintering additives and the SiC nano-inclusions formed *in situ* during the sintering process. Aim of the paper is the study of effect of both SiC inclusions and the chemistry of sintering aids on the room temperature as well as high-temperature properties of this class of ceramics because these have not been reported in the literature yet. This paper tries to find and possibly also explain the relationships between the composition of the sintering additives and the mechanical behaviour of bulk ceramic micro/nano-composites.

2. Experimental procedure

The starting mixtures of the set of six Si_3N_4/SiC micro/nano-composites consisted of the following powders: α-Si_3N_4 (grade SN-E10, UBE Industries, Japan), amorphous SiO_2 (50 $m^2\,g^{-1}$, Aerosil OX-50, Degussa, Germany), carbon black (1000 $m^2\,g^{-1}$, Cabot) and different rare-earth oxides RE_2O_3 (RE = La, Nd, Sm, Y, Yb, or Lu):Y_2O_3 (Pacific Industrial Development Corporation), La_2O_3 (Merck, Germany), Nd_2O_3 (Johnson Matthey GmbH), Sm_2O_3 (Johnson Matthey GmbH), Yb_2O_3 (Pacific Industrial Development Corporation), Lu_2O_3 (Treibacher Industrie AG). All compositions contained the same atomic weight fraction of RE element. Amount of SiO_2 and C was calculated to achieve 5 vol.% of SiC after *in situ* carbothermal reduction process.[11] Simultaneously, the set of six reference monolithic Si_3N_4 materials with the same composition of sintering additives but without SiC nano-inclusions were prepared in order to compare the microstructure and mechanical properties. The raw materials were homogenized and attrition milled in isopropanol for 4 h in polyethylene water cooled bin. The balls and blender were silicon nitride based. The slurries were subsequently dried and the powders sieved through 25 μm sieve. Sieved starting powder was poured into a graphite rectangular die sprayed by thin BN layer from inside. Bulk bodies of 65 mm × 65 mm × 5 mm were then hot-pressed at 1750 °C with a load of 30 MPa and 0.15 MPa pressure of nitrogen during 1 h. Densities were measured by mercury immersion method. The theoretical density was calculated by the rule of the mixtures. Relative densities of all samples were higher than 98% of theoretical density.

Microstructural characterization was carried out using a scanning electron microscopy (SEM) (EVO-40, Zeiss, Germany). Polished sample surfaces were plasma etched using a 1:1 CF_4:O_2 gas mixture in order to reveal the Si_3N_4 grains in the microstructure. Grain diameter (width of the elongated silicon nitride grains) distribution was evaluated by measuring of at least 2300 grains of each sample. The apparent aspect ratio (AR) of the Si_3N_4 grains was obtained by the measurements of grain width and length visualised on the 2D micrographs taken at the magnification of 20 000.

The overall structural and chemical characterization of each specimen was carried out by conventional and analytical TEM investigation with a JEOL-2010 microscope equipped with an ultra-thin window for energy-dispersive X-ray spectrometer.

Bulk ceramic samples were ground to the fine powder in the agate mortar. This powder was used for the identification of crystalline phases using X-ray diffraction (Co Kα radiation, STOE powder diffraction system, Germany).

Hardness measurements were performed on the polished cross-sections of the samples by Vickers hardness tester (LECO LV-100, Leco Co., USA), at 9.8 N load. The sample cross-section perpendicular to the hot-pressing direction was used for Vicker's indentation.

The room temperature bending strength was measured on the 45 mm × 4 mm × 3 mm rectangular bars cut from the hot-pressed bodies with tensile face polished to 3 μm finish at the cross-head speed of 0.5 mm/min and inner/outer span 20/40 mm, respectively. The tensile face of the bars was always perpendicular to the hot-pressed direction.

The Chevron notch technique was used for fracture toughness determination. Chevron notches with the top angle of 90° were introduced into each bar (rectangular cross-section of 3 mm × 4 mm recommended for fracture toughness test by ASTM standard[12]) using an ultra-thin diamond blade on precision saw Isomet 5000. The reliability of this approach was described elsewhere.[13] A universal testing system Instron 8862 equipped with three point bend test fixtures with span of 16 mm was used to apply the loading. A cross-head speed of 10 μm/min was used in all tests to achieve slow crack propagation during loading. An inductive extensometer was used for deflection of measurement and force–deflection curves were recorded. Monitoring of fracture behaviour, mainly crack initiation and subsequently propagation during loading was performed by acoustic emission measurement. The fracture toughness values were calculated from the maximum force (F_{max}) evaluated from the force–deflection curve and the specimen dimension by the following equation[12]:

$$K_{1c} = \frac{F_{max}}{BW^{1/2}Y^*_{min}},$$

where Y^*_{min} is the minimum of geometrical compliance function Y^*, B and W are the width and height of specimens, respectively.

Creep tests were performed in four-point bending using a fixture made of silicon carbide with inner and outer span length of 20 mm and 40 mm, respectively. The measurements were carried out in a creep machine with dead-weight loading system in air atmosphere at temperature between 1250 °C and 1400 °C with outer fiber stresses in the range from 50 MPa to 150 MPa. The sample deflection was recorded continuously during the creep test.

Nitrogen and oxygen content were measured on the powdered samples by the LECO TC-436 analyser in TU Darmstadt.

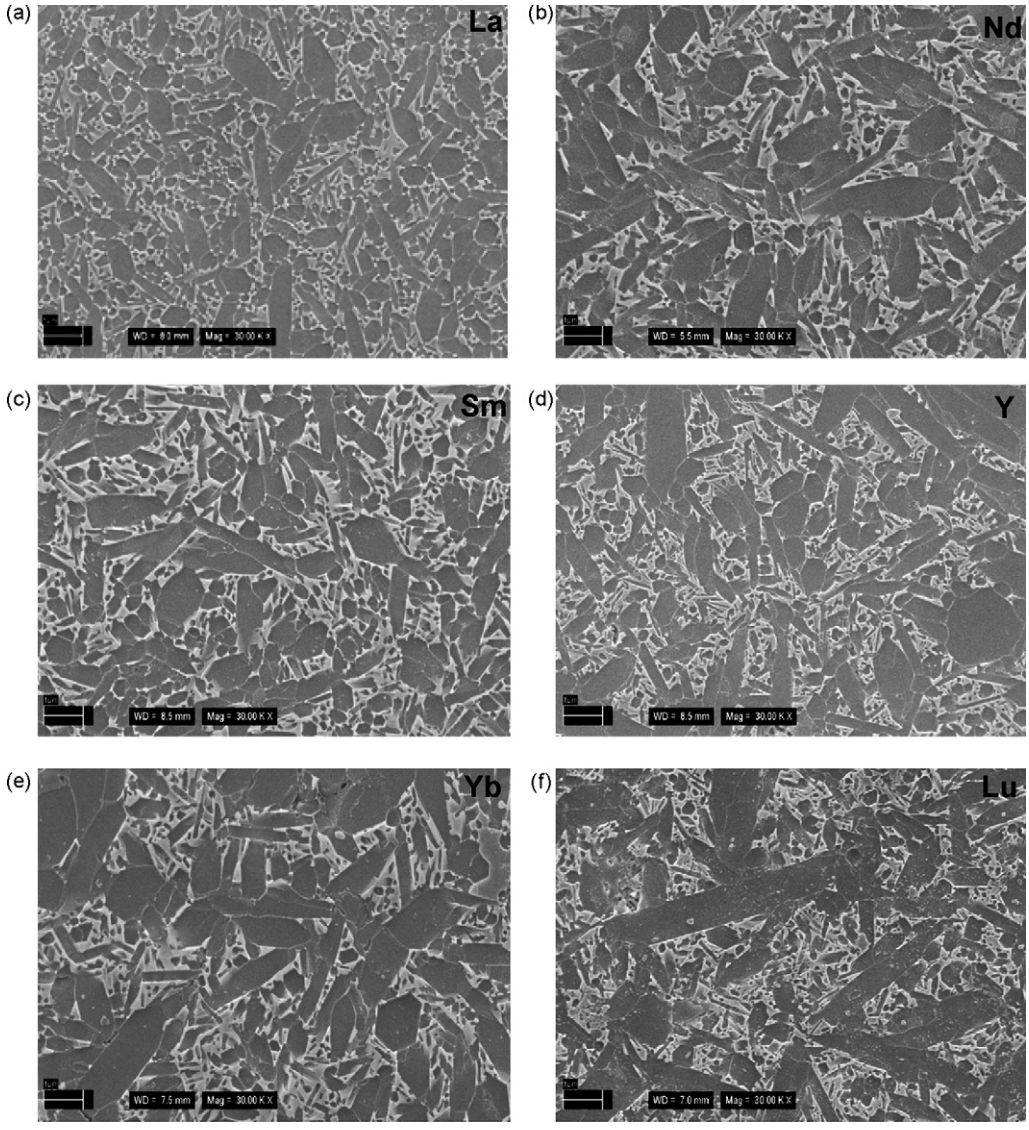

Fig. 1. SEM micrograph of Si_3N_4 containing (a) La_2O_3, (b) Nd_2O_3, (c) Sm_2O_3, (d) Y_2O_3 (e) Yb_2O_3, and (f) Lu_2O_3 additives.

3. Results and discussion

3.1. Microstructural characterization

3.1.1. Monolithic Si_3N_4

The microstructures of the hot-pressed monolithic Si_3N_4 based ceramics with different rare-earth oxides are shown in Fig. 1. It is obvious that these samples have a typical bimodal microstructure composed of large elongated β-Si_3N_4 grains distributed in a fine β-Si_3N_4 matrix. From the micrographs (Fig. 1), it is obvious that the presence of different rare-earth elements in the glassy phase surrounding the silicon nitride grains yields differences in grain growth anisotropy. Samples with small RE^{3+} cations (Yb and Lu) contain larger diameter elongated β-Si_3N_4 grains surrounded by finer β-Si_3N_4 matrix grains typical bimodal distribution (Fig. 1e and f). On the other

Table 1
Crystalline phases in reference materials.

	Reference Si_3N_4			Micro/nano-composite Si_3N_4/SiC				
La	(β)-Si_3N_4	SiO_2	–	(β)-Si_3N_4	SiO_2	SiC	Si_2N_2O	–
Nd	(β)-Si_3N_4	SiO_2	–	(β)-Si_3N_4	SiO_2	SiC	Si_2N_2O	–
Sm	(β)-Si_3N_4	SiO_2	$Sm_{10}(SiO_4)_6N_2$	(β)-Si_3N_4	SiO_2	SiC	Si_2N_2O	$Sm_{10}(SiO_4)_6N_2$
Y	(β)-Si_3N_4	SiO_2	$Y_2Si_2O_7$	(β,α)-Si_3N_4	SiO_2	SiC	Si_2N_2O	$Y_2Si_2O_7$
Yb	(β)-Si_3N_4	SiO_2	?	(β)-Si_3N_4	SiO_2	SiC	Si_2N_2O	$Yb_2Si_2O_7$
Lu	(β)-Si_3N_4	SiO_2	$Lu_2Si_2O_7$	(β,α)-Si_3N_4	SiO_2	SiC	Si_2N_2O	$Lu_2Si_2O_7$

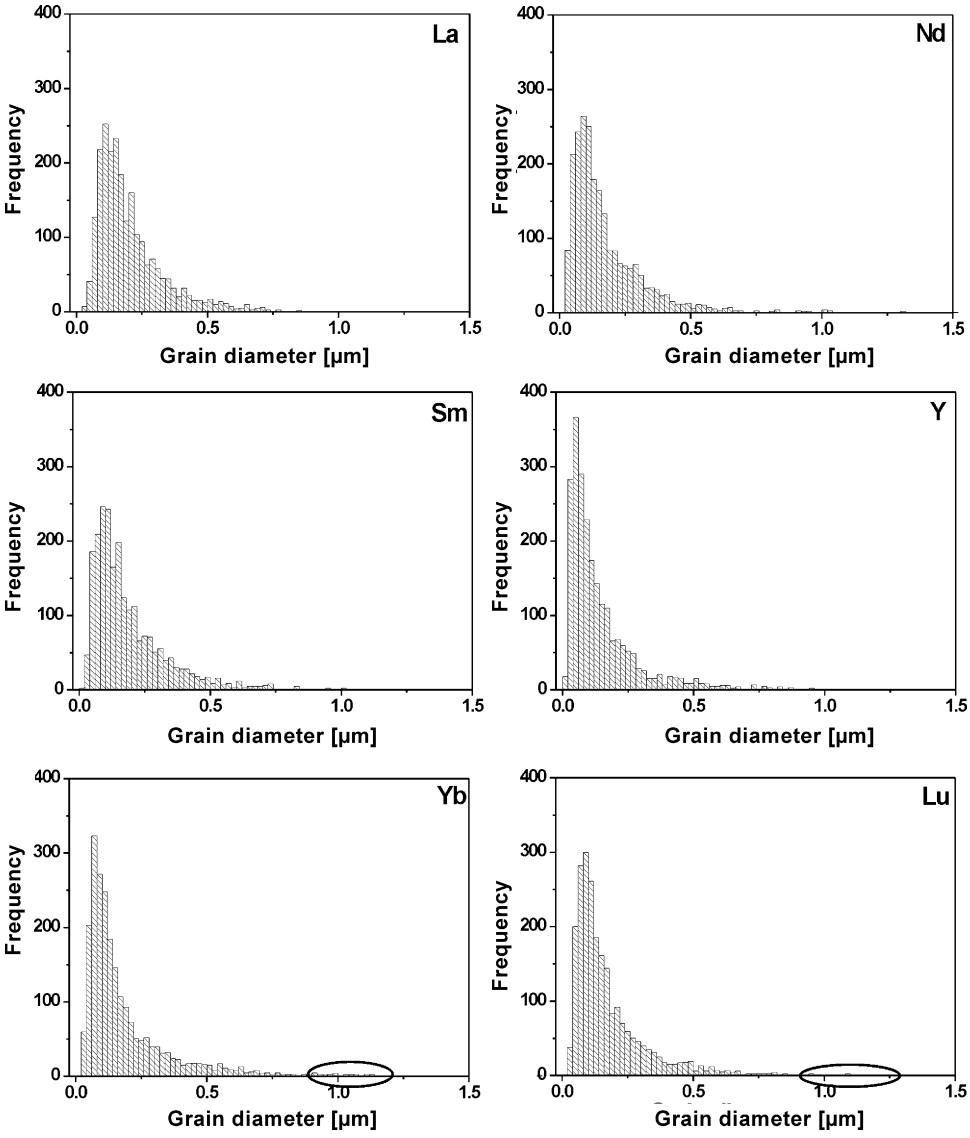

Fig. 2. Grain size distribution of Si_3N_4 grains for the reference monolithic Si_3N_4 materials.

hand samples with large RE^{3+} cations (mainly La, but partly also Nd and Sm) have not express this bimodal distribution so markedly. Grain diameter distributions of all samples are shown in Fig. 2. Higher frequency of appearance of small diameter β-Si_3N_4 matrix grains is evident for Y, Yb, and Lu reference samples. In all these cases the frequency of appearance of grains with small diameter ($d \leq 0.08$ μm) is high, number of counts of these thin grains is ≥300, what is not a case of samples doped by La, Nd and Sm cations. For samples containing Yb and Lu cations also a small number of robust Si_3N_4 grains with the diameter of approx. 1 μm are visible (marked by circles). Apparent aspect ratio as a function of RE^{3+} radius is not changed markedly (Fig. 3). Generally, the tendency of the mean AR is decreasing from Lu cation containing sample to the La cation containing sample.

The explanation of different microstructural evolution of ceramics with various types of oxide additives can be given by

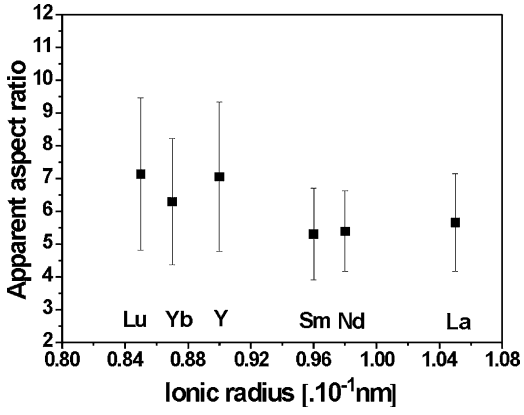

Fig. 3. Aspect ratio of Si_3N_4 as the function of the ionic radius for reference monolithic Si_3N_4 materials.

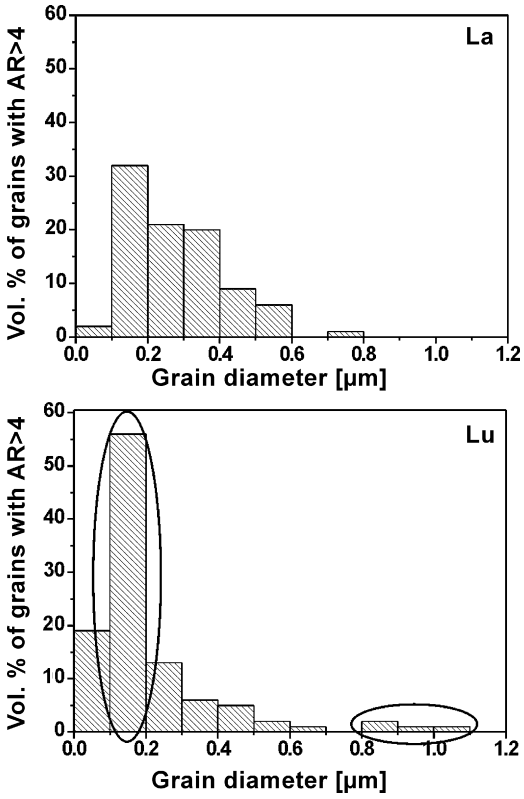

Fig. 4. Volume fraction of grains with AR > 4 for La and Lu reference monolithic Si_3N_4 materials.

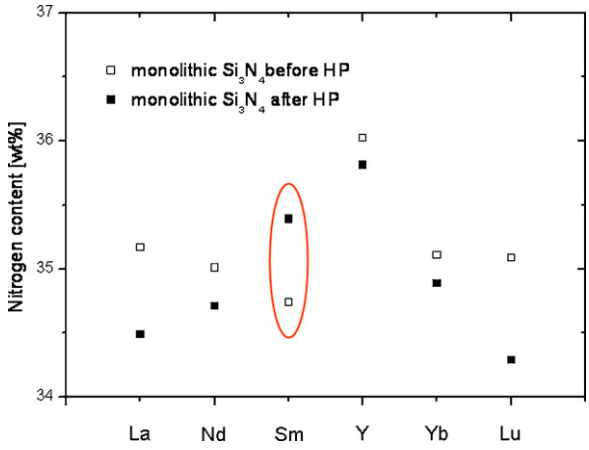

Fig. 5. Nitrogen content in monolithic samples before and after HP cycle.

different viscosities of the liquid phase at the temperature of sintering. It was reported that viscosity of the oxynitride glasses increases with increasing cationic field strength (CFS) and thus decreasing ionic radius of used RE^{3+}.[14–18] Volume fraction of β-Si_3N_4 grains with AR >4 (needle-like grains) for La (the largest RE^{3+}) and Lu (the smallest RE^{3+}) of reference monolithic Si_3N_4 ceramics as the function of the grain diameter is shown in Fig. 4. This graph reveals that Lu reference sample has remarkably higher volume fraction of small needle-like β-Si_3N_4 grains (mean grain diameter <0.2 μm) and slightly higher volume fraction of large needle-like grains (mean grain diameter >0.8 μm) than La sample. An increasing number of small diameter grains with high aspect ratios (Lu sample) are most probably due to the higher viscosity of liquid phase during the sintering temperature. It is supposed that higher viscosity restrains dissolution of silicon nitride grains in the melt with a consequence of lower concentration of ions needed for the precipitation. Moreover, high melt viscosity hinders the material transport by means of diffusion through the liquid.

Different growth of the diameter of pre-existing β-Si_3N_4 grains can be demonstrated by the different tendency of RE elements to segregate on different grain crystallographic surfaces of silicon nitride. Shibata and Ziegler[19,20] reported that La has increasing preference for adsorption on the prismatic grain surfaces (preferred bonding to N), thus impede attachment of Si to the growing interface, which is necessary step for diametric grain growth. Larger diameter of needle-like β-Si_3N_4 grains for Lu sample is explained by higher stability of Lu in the glass (preferred bonding to O), whereby do not impede the attachment of Si and N to the prismatic plane.

XRD analysis shows that α- to β-Si_3N_4 phase transformation was completed after the HP cycle for all sample compositions. Crystalline phases identified by XRD in the sintered samples are listed in Table 1. In Y and Lu contained samples the RE disilicates were identified, in the case of Sm contained sample the apatite phase $Sm_{10}(SiO_4)_6N_2$ was detected. Elemental analysis supports the phase analysis when the nitrogen content of the hot-pressed Sm contained sample was higher compared to the state before hot-pressing. This measurement demonstrates the high solubility of nitrogen in the Sm_2O_3–SiO_2 melt at 1750 °C (Fig. 5) marked by ellipsis. While in La- and Nd-containing samples the secondary crystalline phases were not detected. If there were any present, their content was under the detection limit of used XRD equipment. In the case of Yb doped sample, identification of observed diffraction peaks, probably corresponding to the residual grain boundary phase, has failed.

3.1.2. Si_3N_4/SiC micro/nano-composites

Microstructures of six Si_3N_4/SiC micro/nano-composites sintered with the different rare-earth oxides are shown in Fig. 6. Microstructures consist of elongated Si_3N_4 micrograins and random distributed SiC nano-inclusions. The globular nano (~30 nm) SiC inclusions are located intragranularly within the Si_3N_4 grains; while submicron sized (~150 nm) SiC inclusions are located between the Si_3N_4 grains intergranularly, these are shown by arrows in Fig. 6. Lower viscosity liquid phase (larger RE elements) tends to form intragranular SiC inclusions whereas higher viscosity (smaller RE elements) promotes formation of intergranular SiC inclusions. Evolution of the microstructure of Si_3N_4/SiC micro/nano-composites (Fig. 7) is comparable to the reference monolithic Si_3N_4 materials but generally, the microstructures are finer; this statement is consistent with the assumption that SiC inclusions hindered the grain growth of silicon nitride by grain boundary pinning. Based on the fact that β-Si_3N_4 grain growth is preferential in the *c*-direction,[21,22] the presence of SiC grains hindered silicon nitride grain growth also in this direction and thus influenced an average AR for the composite materials (Fig. 8) which is slightly lower for

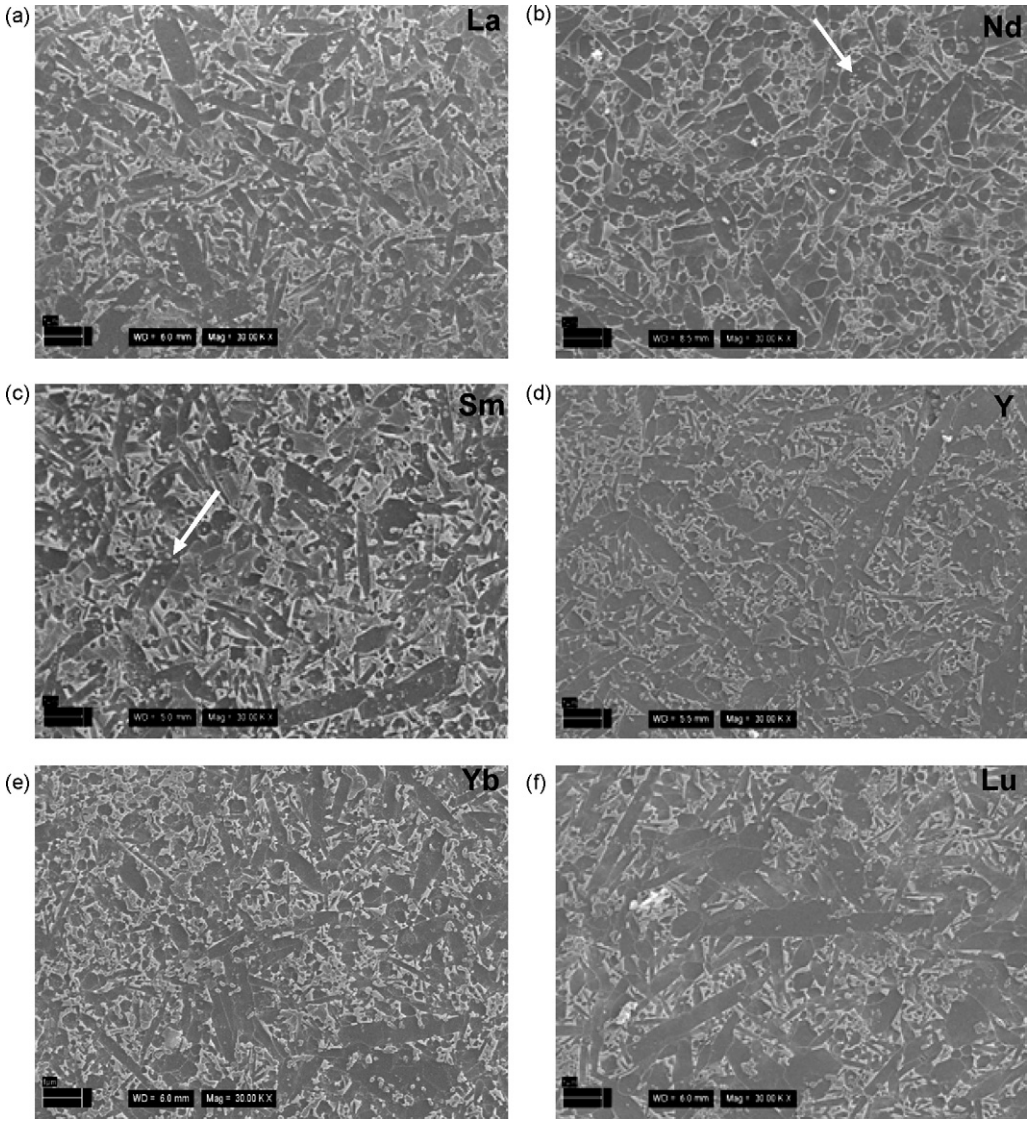

Fig. 6. SEM micrograph of Si_3N_4/SiC micro/nano-composites containing (a) La_2O_3, (b) Nd_2O_3, (c) Sm_2O_3, (d) Y_2O_3 (e) Yb_2O_3, and (f) Lu_2O_3 additives.

all composite samples in comparison to the reference materials.

Table 1 shows that the grain boundary/multigrain junctions crystallised in the phases similar to those observed for monolithic materials. Only substantial difference is a presence of Si_2N_2O in all cases, which means that part of SiO_2 react with Si_3N_4 at the conditions of hot-pressing.

3.2. Room temperature mechanical properties

3.2.1. Fracture toughness of the monolithic Si_3N_4

The fracture toughness measured by Chevron notch bending test of all monolithic samples with different ionic radius of the RE^{3+} oxide sintering additive is shown in Fig. 9. The toughness almost linearly decreases with increasing ionic radius of RE^{3+}. This tendency is in agreement with the decreasing of the apparent aspect ratio of Si_3N_4 grains measured on these samples (Fig. 3).

Higher fracture toughness of the samples with smaller RE elements (Lu, Yb, Y) seems to be a result of the reinforcing effect of the microstructure. Observation of the cracks path (cracks were induced using a Vickers indent at a load of 10 kg) in the La^{3+} and Lu^{3+} containing ceramics showed that crack length of Lu-oxide containing sample is much shorter compared to the La-oxide containing sample (Fig. 10). Higher volume fraction of thin and thick elongated Si_3N_4 grains in Lu-oxide containing sample lead to the higher frequency of the pull-outs and frictional bridges and thus to the more effective dissipation of the crack energy by toughening mechanisms. Šajgalík et al.[23] reported that the highest toughness was obtained for Si_3N_4 ceramics containing high frequency of large reinforcing grains (AR > 4) with the grain diameter >1 μm and/or the high frequency of the small diameter elongated grains (AR > 4). Fig. 4 shows that Lu sample consists of combination of both microstructural reinforcements.

Linear decrease of the fracture toughness from Lu-oxide containing sample to La-oxide containing sample has an exception, this is the Sm-oxide containing sample, characterized by the lowest value of the $K_{1c} = 3.6 \pm 0.31$ MPa $m^{1/2}$. Apatite-type of secondary crystalline phase with the general formula of

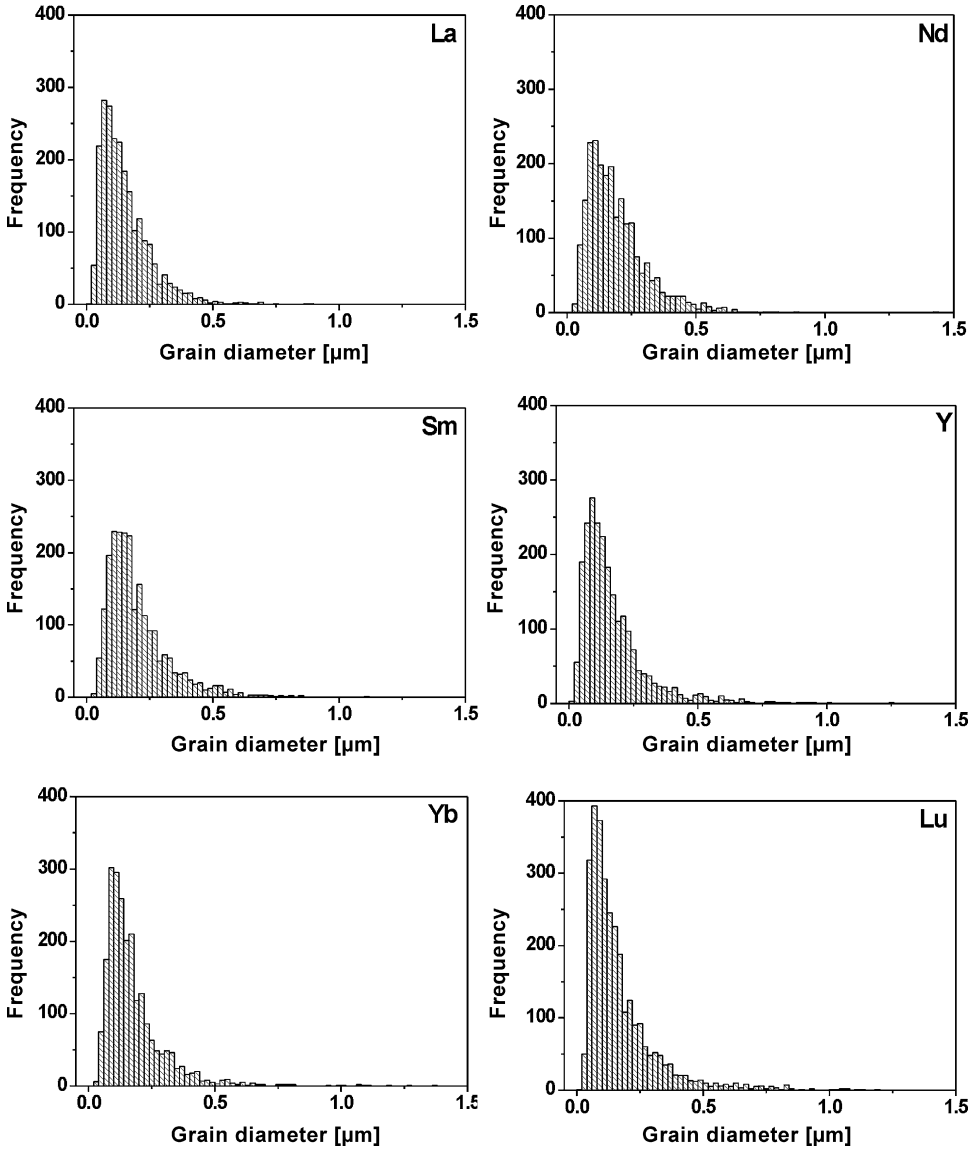

Fig. 7. Grain size distribution of Si_3N_4 grains for the Si_3N_4/SiC micro/nano-composites.

$RE_{10}(SiO_4)_6N_2$ was detected for this sample, Table 1. Generally, apatite-type phase has a coefficient of thermal expansion of $10^{-5}\,K^{-1}$,[24,25] which is much higher in comparison to Si_3N_4, or $RE_2Si_2O_7$. The presence of apatite phase located most probably in the triple points, with approximately three times higher thermal expansion coefficient compared to the major silicon nitride phase results locally in the formation of significant residual (tensile) stresses. These probably negatively influenced the fracture behaviour of such phase containing ceramics at tensile loading.

This result prove the conclusion of many authors that besides the microstructural factors also the phase composition and chemistry of secondary phases significantly affect the composite room temperature fracture behaviour. Many studies of glasses simulating the grain boundary composition of Si_3N_4 based ceramics showed that the mechanical properties (hardness, fracture toughness, Young's modulus, etc.) of glasses doped with RE elements is increasing with the cationic field strength, and/or inversely with the radius of RE^{3+}.[14–18,26,27] These results are consistent with the results of the fracture toughness of bulk Si_3N_4 materials tested in present study.

Satet et al.[1] found out that the fracture toughness of Si_3N_4 sintered with the different rare-earth oxides increases with

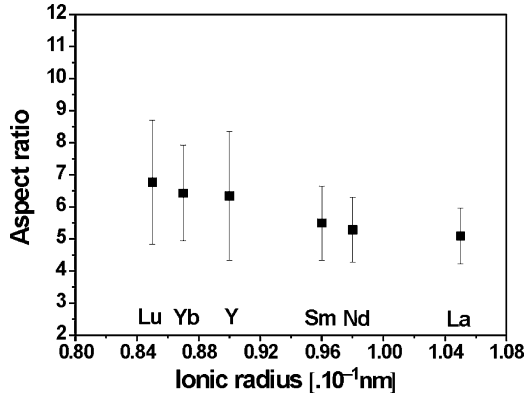

Fig. 8. Aspect ratio of Si_3N_4 as the function of the ionic radius for the Si_3N_4/SiC micro/nano-composites.

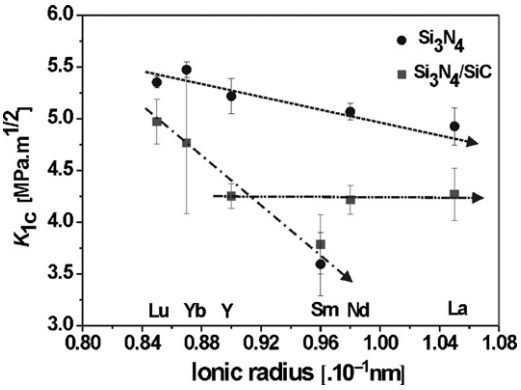

Fig. 9. Fracture toughness of the reference Si_3N_4 and Si_3N_4/SiC micro/nano-composites as the function of rare-earth elements ionic radius.

increasing ionic radius of RE^{3+}. The explanation for this behaviour was given by the higher frequency of pull-out events and frictional bridges as the consequence of the lower interfacial strength when the size of the RE^{3+} cation present in the grain boundary phase increased. This observation is in the contrary to the results presented here, when the fracture toughness decreases with increasing ionic radius of RE^{3+}. There are two possible explanations for this behaviour. The first one is a microstructural aspect and second one is a compositional aspect. In present work the microstructures varied with the addition of different rare-earth oxides, i.e. AR increased from La^{3+} to Lu^{3+} addition. However, Satet et al. made efforts to develop microstructuraly comparable bimodal microstructures for all samples. In their work they varied the sintering conditions (mainly the temperature) in order to obtain the same/similar microstructures for all kinds of RE oxide additives. Nevertheless, their Lu-oxide

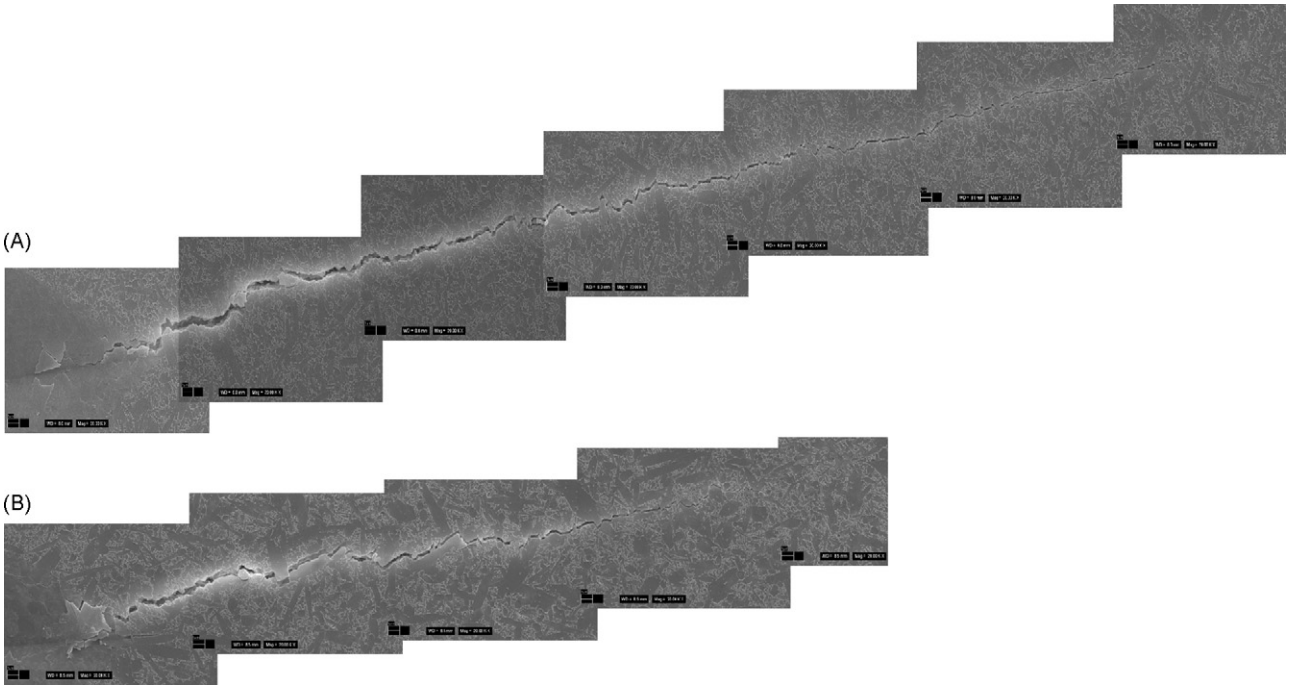

Fig. 10. Crack propagation in the reference monolithic Si_3N_4 materials: (a) La sample and (b) Lu sample.

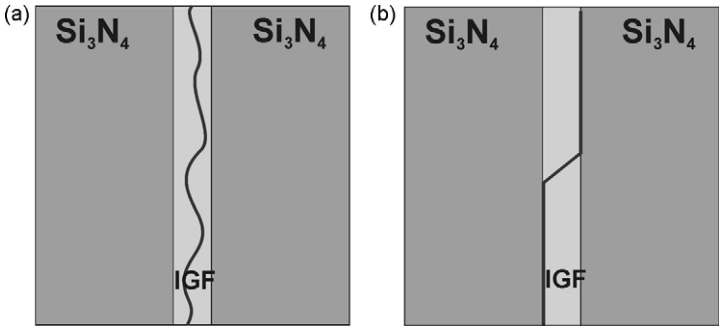

Fig. 11. Hypothetically possible ways of crack paths: (a) crack propagation within the IGF and (b) crack propagating through interface between Si_3N_4 grain and IGF.

containing sample displayed higher AR in comparison with the other samples, but K_{1c} measured for this composition was the lowest of all. This indicates that the compositional aspect, also in their case, seems to be more important than the microstructural. Satet et al. used MgO as the sintering additive in addition to the SiO_2 and RE_2O_3. However, adsorption sites of REs on the Si_3N_4 grain surface were studied and it is believed that their location is known. On the other hand, location of Mg in the nanometer-thick intergranular film (IGF) and/or grain/IGF interface have not been investigated yet. Understanding the nature of the bonding within the IGF and along the interface between the Si_3N_4 grain/IGF in ceramics with different composition of the additives is required to give appropriate explanation for the crack propagation. For example, Becher et al.[28] observed that increase of the Y/Al ratio in self-reinforced silicon nitride with Si–Al–Y oxynitride glass promotes debond path within the IGF due to the weakening of the glassy phase. Fig. 11 shows a schematic picture of hypothetically possible ways of crack paths: (a) crack propagation within the IGF and (b) crack propagating through interface between Si_3N_4 grain and IGF (interfacial debonding). It can be deduced that in case (a) when the crack path run through the IGF, the fracture behaviour of ceramics should be dictated by the properties of the residual glass. In present case, the fracture toughness of RE doped ceramics decreases with increasing ionic radius of RE^{3+} in residual glass. This decreasing trend of ceramics is consistent with the dependence of fracture toughness of glasses doped by the RE elements.[27] By this similarity, it can be concluded that in present case the crack most probably propagates within the IGF in reference Si_3N_4 based ceramics and the toughness of the bulk material is dictated by the properties of glassy phase and not by the strength of the bond between Si_3N_4 grain and IGF. This fracture, which is dependent on the glassy phase composition, can be one of the reasons for the dissimilarities in the fracture behaviour of samples prepared by Satet et al.[1] The knowledge of chemical composition and the structure of the IGF are crucial for this idea. The deep research of IGF with the thickness $\leq$1 nm is necessary. This investigation is rather problematic not only because of technical difficulties but also because of questionable reliability of the data obtained from a limited number of HRTEM micrographs. The first principle calculations coupled with HRTEM analysis could put more light to this problem.[19]

3.2.2. *Fracture toughness of the Si_3N_4/SiC micro/nano-composites*

Generally, for all prepared composite samples the measured fracture toughness values are slightly lower in comparison with the reference monolithic silicon nitride materials (Fig. 9). One of the plausible explanations of this observation can be attributed to finer microstructures with the lower values of mean aspect ratio of elongated grains in Si_3N_4/SiC composites and thus lower effectivity of the toughening mechanisms as crack bridging and/or whisker pull-out compared to the monolithic ceramics. The comparison of fracture toughness of Si_3N_4/SiC micro/nano-composites and monolithic Si_3N_4 ceramics shows differently shaped dependence (stressed by the dashed arrows in Fig. 9) with respect to the size of ionic radius of used RE^{3+}. The fracture toughness of Si_3N_4/SiC micro/nano-composites containing

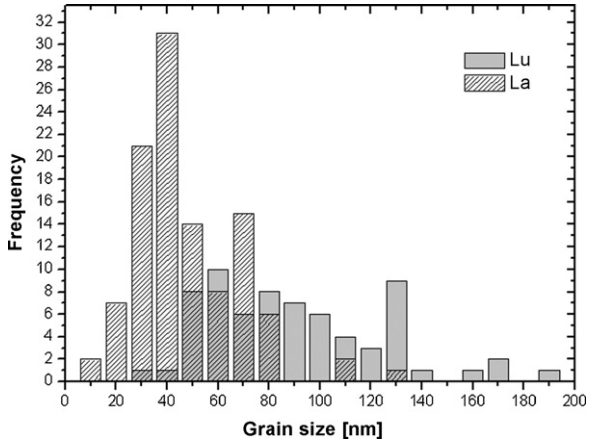

Fig. 12. SiC grain size distribution in the La and Lu doped Si_3N_4/SiC micro/nano-composites.

Lu^{3+}, Yb^{3+} and Y^{3+} linearly decreases from 5.0 MPa $m^{1/2}$ for Lu^{3+} containing sample to 4.2 MPa $m^{1/2}$ for Y^{3+} containing sample. Even Sm^{3+} containing sample apparently follows this tendency. Samples containing Nd- and La-oxide additives are different, their values of fracture toughness are similar and more or less the same as for the Y^{3+} containing sample. It seems that the fracture behaviour of Si_3N_4/SiC micro/nano-composites is influenced by the presence of SiC nano-inclusions. It was observed that the distribution of SiC nano-inclusions within the RE-oxide doped micro/nano-composites is different. Fig. 12 shows the size distribution of the SiC grains obtained from the TEM micrographs. The number of analysed SiC grains is limited (72 grains for Lu doped sample and 111 grains for La doped sample) but some trends can be seen. La contained samples produces much higher number of small SiC grains with the average size of 44 nm while Lu doped sample has an average size of SiC grains almost doubled, 77 nm. Finer SiC grains in La doped samples indicate higher nucleation rate of SiC in the La_2O_3–SiO_2 melt compared to Lu_2O_3–SiO_2 melt.

From the microstructural observations it can be concluded that lower viscosity of liquid phase (larger RE elements) predominantly leads to the formation of *intra*-SiC inclusions and higher viscosity (smaller RE elements) leads to the formation of *inter*-SiC, as it is documented on the micrograph in Fig. 13. The lower viscosity promotes solution–reprecipitation process and the growth of β-Si_3N_4 grains. However, the growth of β-Si_3N_4 grains is hindered by the presence of SiC nano-inclusions but the low viscosity liquid diminishes the interfacial energy, which is beneficial for the entrapping of the smallest SiC inclusions in the β-Si_3N_4 host grain.[29] Higher fraction of intragranular SiC was observed for La- and Nd-oxide doped samples compared to the Lu- and Yb-oxide doped samples. The higher concentration of *intra*-SiC probably restrains the microstructural and/or compositional effect on the fracture toughness and consequently the decreasing tendency of toughness stopped for the La- and Nd-oxide doped samples. It was reported[30,31] that SiC inclusions distributed in Si_3N_4 matrix have a positive effect on the fracture toughness because of the formation of significant residual stresses within the silicon nitride matrix caused by the differ-

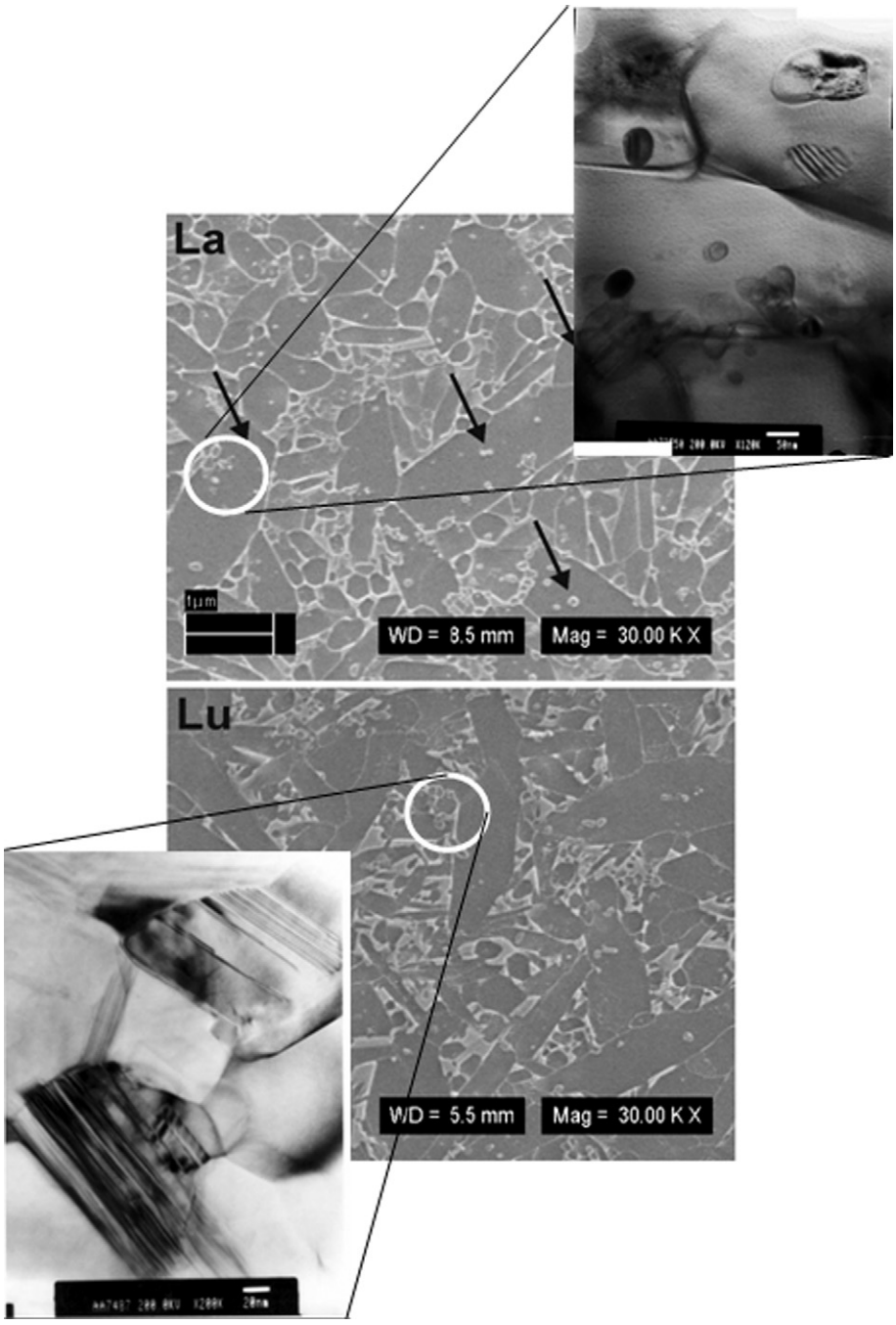

Fig. 13. Distribution of SiC in La^{3+} and Lu^{3+} cations containing composite samples.

ent thermal expansion coefficient of these two phases. Lower fracture toughness of composite materials presented here indicates that *intra*-SiC nano-inclusions with an oxygen rich surface layer[11] created by the carbothermal reduction of SiO_2 with carbon during the sintering process helped to relax the stresses around the SiC inclusions and hence decreased the positive influence of SiC nano-inclusions on the fracture toughness. The lowest difference in K_{1c} values of Lu-oxide doped reference and composite samples compared to other compositions lead to the assumption that higher frequency of *inter*-SiC inclusions in Lu-oxide doped micro/nano-composite has a positive effect on fracture toughness because of the higher incidence of crack impediment events. Crack can be deflected by the intergranular SiC inclusions.

3.2.3. Hardness of the monolithic Si_3N_4

Fig. 14 shows the hardness as the function of ionic radius of all monolithic Si_3N_4 materials. Hardness decreases with increasing ionic radius of RE^{3+} from 17.0 ± 0.40 GPa for Lu-oxide containing sample to 15.4 ± 0.14 GPa for La-oxide containing sample. This dependence documents the fact that the chemical composition of secondary phases in ceramics has a strong influence also on the microhardness of ceramics. This observation is in agreement with the findings of other authors.[32–34]

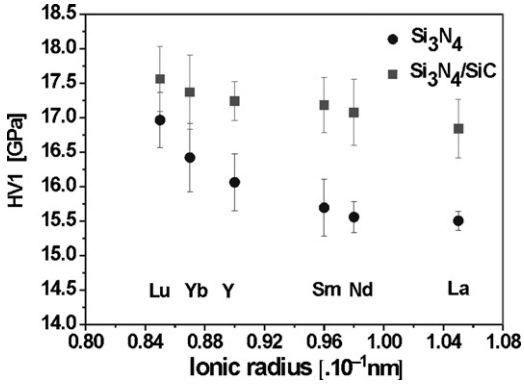

Fig. 14. Hardness of the reference Si_3N_4 and Si_3N_4/SiC micro/nano-composites as the function of rare-earth elements ionic radius.

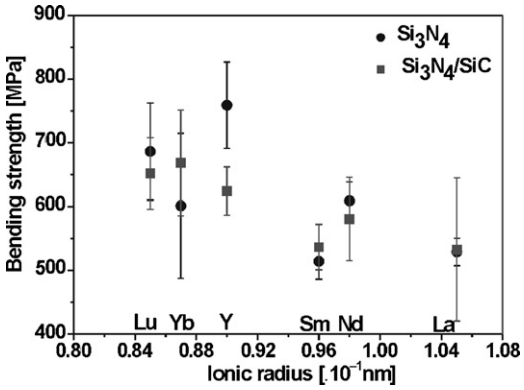

Fig. 15. Strength of the reference Si_3N_4 and Si_3N_4/SiC micro/nano-composites as the function of rare-earth elements ionic radius.

3.2.4. Hardness of the Si_3N_4/SiC micro/nano-composites

The hardness values of Si_3N_4/SiC micro/nano-composites as a function of the ionic radius used RE^{3+} are also depicted in Fig. 14. The hardness values of Si_3N_4/SiC composite materials are higher compared with SiC-free monolithic Si_3N_4 materials. Similarly to monoliths also in this case the hardness decreases with increasing ionic radius of used RE^{3+} from 17.6 ± 0.47 GPa for Lu-oxide containing sample to 16.8 ± 0.43 GPa for La-oxide containing sample.

This slight increase of hardness of micro/nano-composites compared to the monoliths can be attributed to both, microstructural and compositional effect. Materials with a finer microstructure usually have higher hardness because of Hall–Petch effect[35,36] referring the restricted dislocation mobility in smaller grains. On the other hand, higher hardness of β-SiC single crystal compared to β-Si_3N_4 single crystal positively affected the microhardness values of Si_3N_4/SiC micro/nano-composites. Distribution of SiC nano-inclusions in the microstructure seems to be also an important factor for microhardness of ceramic micro/nano-composites. The hardness values of Lu-oxide containing samples for the reference and composite materials are 17.6 ± 0.47 GPa and 17.0 ± 0.40 GPa, respectively; the difference 0.60 GPa is almost in the range of experimental error. The hardness values of La-oxide containing monolithic and composite samples are 16.8 ± 0.43 GPa and 15.4 ± 0.14 GPa, respectively; the difference between them 1.4 GPa is significant. This observation and the fact that the microstructure of La^{3+} doped composite sample contains mainly SiC *intra*-inclusions indicate the importance of the SiC nano-inclusions distribution. Their presence within the Si_3N_4 grain increases the nanohardness of this grain itself not only by higher hardness of SiC nano-inclusion, but also by creation of sub-grain boundaries[37] which allow to act the Hall–Petch effect on this sub-grain level. In this case, the effect of the chemical composition of the grain boundaries is lower and thus the slope of *HV1* in composites is smaller compared to monoliths.

3.2.5. Strength of the monolithic Si_3N_4

The four-point bending strength as a function of the ionic radius used RE^{3+} for monolithic Si_3N_4 ceramics is shown in Fig. 15. Mean values of the strength of all samples are in the range of 759 ± 68 MPa for the Y-oxide containing sample and 514 ± 28 MPa for the Sm-oxide containing sample. The low value of the strength of Sm-oxide containing sample can be attributed to the presence of the apatite phase with high thermal expansion coefficient and the thus negative influence of residual stresses in this particular sample are predictable. The highest scatter of measured values was determined for the Yb-oxide containing sample, the lowest for the La-containing sample.

3.2.6. Strength of the Si_3N_4/SiC micro/nano-composites

The strength of composite materials is given in Fig. 15 as a function of the ionic radius of used RE^{3+}. The strength decreases with increasing ionic radius of RE^{3+}: from 668 ± 83 MPa for Yb-oxide containing sample to 532 ± 112 MPa for La-oxide containing sample.

In majority cases as a crack origins the residual carbon areas as well as agglomerates of SiC were detected, similarly to the materials investigated in the previous work of the authors.[38]

Fig. 15 shows that the bending strength of monoliths and micro/nano-composites decrease with the increasing radius of RE^{3+}. The processing of all samples was the same and thus it can be assumed that in all cases the critical defects were on the same size level. If this assumption is correct, then according to the Griffit's theory the strength is directly proportional to the fracture toughness. For both series of samples, monolithic as well as composite ones the decrease of fracture toughness values from Lu^{3+} to La^{3+} doped samples was observed in present work. The strength values follow the same tendency.

3.3. High-temperature mechanical properties

3.3.1. Creep resistance

The creep resistance was studied only for materials containing a sintering additive with the smallest and the largest ionic radius of RE^{3+}. These experiments were performed for Lu and La containing reference Si_3N_4 monolithic and Si_3N_4/SiC micro/nano-composite samples. The strain-time dependencies of La-oxide and Lu-oxide containing reference and composite samples, respectively at 1350 °C and stress of 100 MPa are shown in Fig. 16. Whereas, the reference monolithic Lu-oxide containing sample is characterized by nearly 1% strain

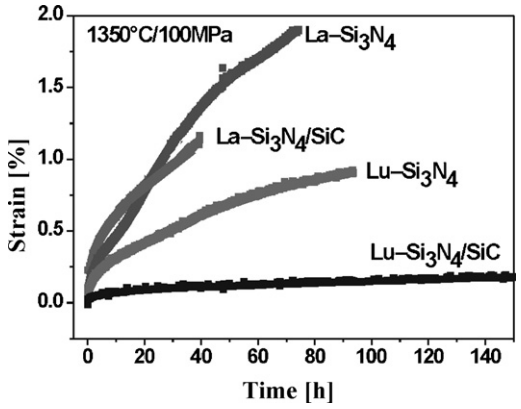

Fig. 16. Creep deformation at 1350 °C and stress of 100 MPa of La and Lu reference and composite samples.

at 1350 °C, the composite Lu-oxide containing sample shows negligible strain change. The difference in strain is smaller for both La-oxide containing monolithic Si_3N_4 and Si_3N_4/SiC micro/nano-composite. The creep rate at 1300 °C is almost 1 order of magnitude lower for Lu-oxide containing micro/nano-composite compared to the Lu-oxide containing monolithic sample and almost 2 orders of magnitude lower than La-oxide containing both monolithic and composite materials, Fig. 17. The slopes of strain–stress dependencies of La-oxide and Lu-oxide containing micro/nano-composites at 1350 °C are close to 1 (Fig. 18), indicating that the diffusion is the main creep mechanism.[9,10]

Also in the case of high-temperature deformation of micro/nano-composites the *intra*/*inter*-SiC nano-inclusions distribution is a dominant for their behaviour. It was supposed and by Figs. 13 and 16 it is documented that *inter*-SiC inclusions will play much more decisive role than *intra*-SiC. While for monolithic and composite material containing La-oxide additives the deformation curves are similar, the strain of the Lu-oxide containing sample is much lower in the case of micro/nano-composite. The role of intergranular SiC inclusions is obvious. Fig. 19 strongly supports this statement while in the case of Lu doped samples the residual content of oxygen is almost the same for both reference and micro/nano-composite samples and thus

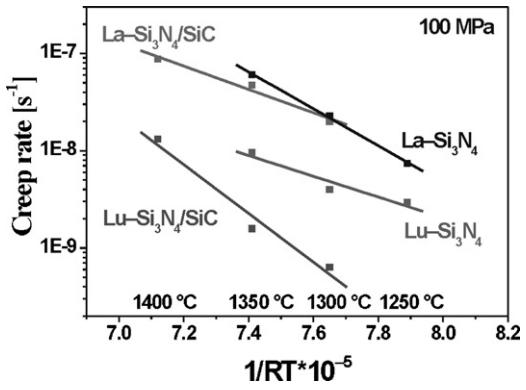

Fig. 17. Comparison of creep rate for La and Lu reference and composite samples.

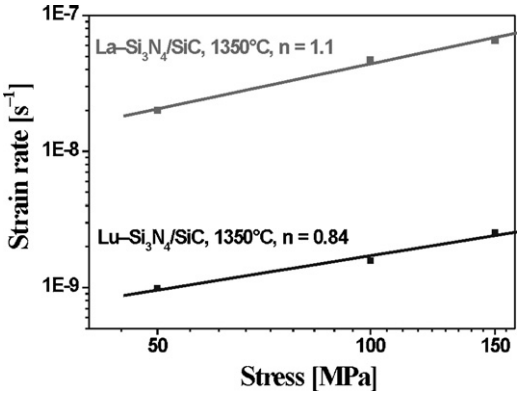

Fig. 18. Strain rate–stress dependence of La and Lu composite samples.

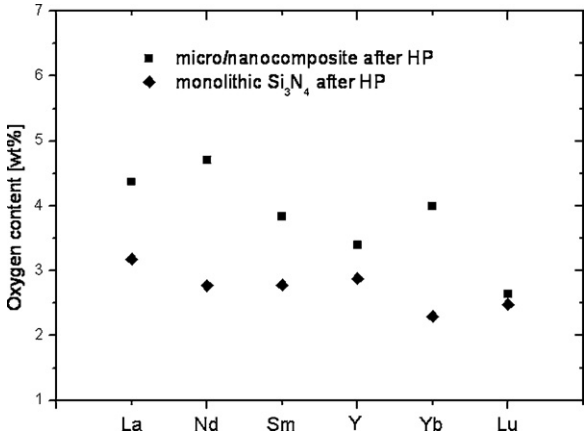

Fig. 19. Oxygen content in both, reference Si_3N_4 and Si_3N_4/SiC micro/nano-composites after HP cycle.

only difference from the chemical point of view is the distribution of intragranular SiC inclusions in the microstructure.

Viscosity of the glassy phase decreases with the increasing temperature and softened intergranular glassy phase leads to the grain-boundary sliding and consequently to the material deformation. SiC inclusions distributed along the grain boundaries limit the grain-boundary sliding and hence improve creep resistance. The highest creep resistance achieved for Lu-oxide containing composite material is attributed to a positive effect of *inter*-SiC inclusions and compositional aspect of the intergranular phase. Intergranularly distributed SiC nano-inclusions hinder the grain-boundary sliding as it was previously published by the authors.[9,10]

4. Conclusions

The influence of the intergranular phase composition on mechanical properties of Si_3N_4/SiC micro/nano-composites has been investigated using SiO_2 and RE_2O_3 (RE = La, Nd, Sm, Y, Yb, or Lu) as the sintering additives. Impact of the composition of the intergranular phase on the formation of SiC has also been studied. The properties were compared with reference monolithic Si_3N_4 material with the same composition of intergranular glassy phase.

The fracture toughness, hardness and strength of the reference monolithic Si_3N_4 and Si_3N_4/SiC composite materials showed decreasing tendency with the increasing radius of RE^{3+}. Distribution of SiC nano-inclusions influenced the room temperature mechanical properties of Si_3N_4/SiC micro/nano-composites in the sense that *intra*-SiC nano-inclusions decrease the fracture toughness but increase the hardness. The creep resistance of Si_3N_4/SiC micro/nano-composites is improved by *inter*-SiC nano-inclusions. Intergranularly located SiC nano-inclusions hinder the grain-boundary sliding. The distribution of SiC in Si_3N_4 matrix was probably influenced by the different viscosity of liquid phase at sintering temperature; the viscosity decreases with increasing ionic radius of RE^{3+} in the order of quotation. Lower viscosity of liquid phase predominantly lead to the formation of *intra*-SiC inclusion and higher viscosity lead to the formation of *inter*-SiC.

The best creep resistance was observed for Lu-based composite material. This material has the highest creep resistance, the highest hardness and reasonably high fracture toughness and strength.

Acknowledgements

This work was supported by the Slovak Grant Agency VEGA Project No. 2/7171/27, APVV-0171-06, Centrum of Excellence NANOSMART. Author S.L. acknowledge Prof. Ralf Riedel for the possibility to make the nitrogen/oxygen analysis at TU Darmstadt.

References

1. Satet RL, Hoffmann MJ. Influence of the rare-earth element on the mechanical properties of RE–Mg-bearing silicon nitride. *J Am Ceram Soc* 2005;**88**:2485–90.
2. Satet RL, Hoffmann MJ, Cannon RM. Experimental evidence of the impact of rare-earth elements on particle growth and mechanical behaviour of silicon nitride. *Mater Sci Eng A* 2006;**422**:66–76.
3. Guo S, Hirosaki N, Yamamoto Y, Nishimura T, Kagawa Y. Hot-pressed Si_3N_4 ceramics with Lu_2O_3 additives: grain-boundary phase and strength. *Mater Sci Eng A* 2005;**408**:9–18.
4. Choi H-J, Lee J-G, Kim Y-W. High temperature strength and oxidation behaviour of hot-pressed silicon nitride–disilicate ceramics. *J Mater Sci* 1997;**32**:1937–42.
5. Cinibulk MK, Thomas G. Oxidation behavior of rare-earth disilicate–silicon nitride ceramics. *J Am Ceram Soc* 1992;**75**:2044–9.
6. Cinibulk MK, Thomas G. Strength and creep behavior of rare-earth disilicate–silicon nitride ceramics. *J Am Ceram Soc* 1992;**75**:2050–5.
7. Lofaj F, Wiederhorn SM, Long GG, Hockey BJ, Jemian PR, Bowder L, et al. Non-cavitational tensile creep in Lu-doped silicon nitride. *J Eur Ceram Soc* 2002;**22**:2479–87.
8. Niihara K. New design concept of structural ceramics–ceramics nanocomposites. *J Jpn Ceram Soc* 1991;**99**:974–82.
9. Šajgalík P, Hnatko M, Lofaj F, Hvizdoš P, Dusza J, Warbichler P, et al. SiC/Si_3N_4 nano/micro-composite processing, RT and HT mechanical properties. *J Eur Ceram Soc* 2000;**20**:453–60.
10. Dusza J, Kovalčík J, Hvizdoš P, Šajgalík P, Hnatko M, Reece M. Creep behavior of a carbon-derived Si_3N_4/SiC nanocomposite. *J Eur Ceram Soc* 2004;**24**:3307–15.
11. Hnatko M, Galusek D, Šajgalík P. Low-cost preparation of Si_3N_4–SiC micro/nano composites by in-situ carbothermal reduction of silica in silicon nitride matrix. *J Eur Ceram Soc* 2004;**24**:189–95.
12. *ASTM C1421, standard test method for determination of fracture toughness of advanced ceramics at ambient temperature*; 2002.
13. Boccaccini AR, Rawlings RD, Dlouhy I. Reliability of the chevron-notch technique for fracture toughness determination in glass. *Mater Sci Eng A* 2003;**347**:102–8.
14. Lofaj F, Satet R, Hoffmann MJ, López AR. Thermal expansion and glass transition temperature of rare-earth doped oxynitride glasses. *J Eur Ceram Soc* 2004;**24**:3377–85.
15. Lofaj F, Dériano S, LeFloch M, Rouxel T, Hofmann MJ. Structure and rheological properties of the RE–Si–Mg–O–N (RE = Sc, Y, La, Nd, Sm, Gd, Yb and Lu) glasses. *J Non-Cryst Solids* 2004;**344**:8–16.
16. Ramesh R, Nestor E, Pomeroy MJ, Hampshire S. Formation of Ln–Si–Al–O–N glasses and their properties. *J Eur Ceram Soc* 1997;**17**:1933–9.
17. Hampshire S. Oxynitride glass, their properties and crystallization—a review. *J Non-Cryst Solids* 2003;**316**:64–73.
18. Becher P, Ferber MK. Temperature-dependent viscosity of SiREAl-based glasses as a function of N:O and RE:Al ratios (RE = La, Gd, Y, and Lu). *J Am Ceram Soc* 2004;**87**:1274–9.
19. Shibata N, Painter GS, Satet RL, Hoffmann MJ, Pennycook SJ, Becher PF. Rare-earth adsorption at intergranular interface in silicon nitride ceramics: subnanometer observation and theory. *Phys Rev B* 2005;**72**:140101–4.
20. Ziegler A, Idrobo JC, Cinibulk MK, Kisielowski C, Browning ND, Ritchie RO. Interface structure and atomic bonding characteristics in silicon nitride ceramics. *Science* 2004;**306**:1768–70.
21. Krämer M, Hoffmann MJ, Petzow G. Grain growth studies of silicon nitride dispersed in an oxynitride glass. *J Am Ceram Soc* 1993;**76**:2778–84.
22. Kramer M, Wittmuss D, Kuppers H, Hoffmann MJ, Petzow G, Lofaj F. Relations between crystal structure and growth morphology of β-Si_3N_4. *J Cryst Growth* 1994;**140**:157–66.
23. Šajgalík P, Dusza J, Hoffmann MJ. Relationship between microstructure, toughening mechanisms, and fracture toughness of reinforced silicon nitride ceramics. *J Am Ceram Soc* 1995;**78**:2619–24.
24. Sun Z, Li M, LI Z, Zhou Y. Hot corrosion of γ-$Y_2Si_2O_7$ in strongly basic Na_2CO_3 molten salt environment. *J Eur Ceram Soc* 2008;**28**:259–65.
25. Mitomo M, Izumi F, Horiuchi S, Matsui Y. Phase relationships in the system Si_3N_4–SiO_2–La_2O_3. *J Mater Sci* 1982;**17**:2359–66.
26. Becher PF, Waters SB, Westmoreland CG, Riester L. Compositional effect on the properties of Si–Al–RE-based oxynitride glasses (Re = La, Nd, Gd, Y, or Lu). *J Am Ceram Soc* 2002;**85**:897–902.
27. Lofaj F, Satet R, Hoffmann MJ, Dorčáková F, Arellano, Lopéz AR. Rheological properties of the rare earth doped glasses. *Key Eng Mater* 2004;**264-268**:1867–70.
28. Becher PF, Painter GS, Lance MJ, Li S, Ikuhara Y. Direct observations of debonding of reinforcing grains in silicon nitride ceramics sintered with yttria plus alumina additives. *J Am Ceram Soc* 2005;**88**:1222–6.
29. Šajgalík P, Dusza J, Lenčéš Z, Hnatko M, Galusek D, Ghillányová K. Bulk ceramic nanocomposites. In: Riedel R, Chen I-W, editors. *Ceramic science and technology*, vol. 1. KGaA, Weinheim: Wiley-VCH GmBH & Co.; 2008. p. 347–75.
30. Rouxel t, Wakai F, Brito ME, Iwamoto A, Izaki K. Intragranular crack deflection and slip in Si_3N_4/SiC nano-composites crystallographic. *J Eur Ceram Soc* 1993;**11**:431–8.
31. Šajgalík P, Hnatko M, Lenčéš Z. Properties of silicon nitride/carbide nano/micro composites—role of SiC nanoinclusions and grain boundary chemistry. In: Heinrich G, Aldinger F, editors. *Ceramic materials and components for engines*. Weinheim/New York/Chichester/Singapore/Toronto: Wiley-VCH; 2001. p. 553–8.
32. Zemanová M, Lecomte E, Šajgalík P, Riedel R. Polysilazane derived micro/nano Si_3N_4/SiC composites. *J Eur Ceram Soc* 2002;**22**:2963–8.
33. Balog M, Šajgalík P, Lenčéš Z, Kečkeš J, Huang JL. Liquid phase sintering of SiC with AlN and rare earth additives. In: Brito ME, Lin H-T, Plucknett K, editors. *Silicon-based structural ceramics for the new millennium, Ceramic transactions*, vol. 142. 2003. p. 191–202.

34. Balog M, Šajgalík P, Hnatko M, Lenčéš Z, Monteverde F, Kečkéš J, et al. Nano-versus macro-hardness of liquid phase sintered SiC. *J Eur Ceram Soc* 2005;**25**:529–34.
35. Hall EO. The deformation and ageing of mild steel. 3. Discussion of results. *Proc Phys Soc London Sect B* 1951;**64**:747–53.
36. Petch NJ. The cleavage strength of polycrystals. *J Iron Steel Inst* 1953;**174**:25–8.
37. Šajgalík P, Rajan K, Riedel R. Sub grain boundary formation in Si_3N_4 based ceramics. *Key Eng Mater* 1999;**161–163**:229–34.
38. Kašiarová M, Dusza J, Hnatko M, Šajgalík P, Reece MJ. Fractographic montage for a Si_3N_4–SiC nanocomposite. *J Am Ceram Soc* 2006;**89**:1752–5.